Risk-aware Trajectory Planning in Urban Environments with Safe Emergency Landing Guarantee

Jakub Sláma Petr Váňa Jan Faigl

***Abstract*— In-flight aircraft failures are never avoidable entirely, inducing a significant risk to people and properties on the ground in an urban environment. Existing risk-aware trajectory planning approaches minimize the risk by determining trajectories that might result in less damage in the case of failure. However, the risk of the loss of thrust can be eliminated by executing a safe emergency landing if a landing site is reachable. Therefore, we propose a novel risk-aware trajectory planning that minimizes the risk to people on the ground while an option of a safe emergency landing in the case of loss of thrust is guaranteed. The proposed method has been empirically evaluated on a realistic urban scenario. Based on the reported results, an improvement in the risk reduction is achieved compared to the shortest and risk-aware only trajectory. The proposed risk-aware planning with safe emergency landing seems to be suitable trajectory planning for urban air mobility.**

I. Introduction

Although aircraft are one of the safest means of transportation, a failure may happen unexpectedly at any time. Any in-flight failure is not a threat only to the crew and passengers but also to people and properties on the ground. The chance of casualties and material damage on the ground in the case of a crash in rural areas is low, but it is significantly increased in an urban environment due to high population density. Thus, flying over cities is restricted to aircraft with specific capabilities reducing the probability of crashes inside the city. The usage of small aircraft for personal transportation, so-called urban air mobility, is rising, and one may expect the increase of air traffic in urban environments will continue [1].

The risk due to possible crashes can be defined in various ways ranging from the economic evaluation to the number of casualties [2], [3]. Regardless of the definition, proper trajectory planning may reduce the risk. In [4], it is reported that the general aviation accident rate was 5.78 accidents per 10^5 flight hours in the U.S. in 2014. Approx. 75 % of those accidents were caused by a pilot mistake, mechanical issues caused about 15 % of those, and others, e.g., severe weather, caused the remaining 10 %. Note that only accidents with substantial damage were recorded. Therefore, trajectory planning may play a crucial role in reducing the risk of possible in-flight failure and subsequent crashes.

On the other hand, not all in-flight failures lead to a crash. For example, an emergency landing can be performed in the total Loss of Thrust (LoT) incident if a landing site is within a gliding range of the aircraft. According to [5], an engine failure rate was 13 failures per 10^5 flight hours in Australia between 2009 and 2014, which is also higher than the recorded accident rate. Therefore, an aircraft may be required to fly only in areas allowing a safe emergency landing to mitigate the risk induced by LoT [6].

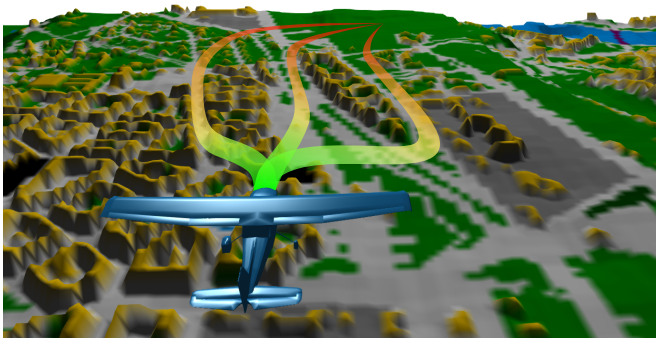

Fig. 1. Visualization of the problem of finding a trajectory with minimal risk of casualty on the ground in the case of an in-flight failure. If an aircraft falls, it poses a risk to people and properties on the ground. Thus, trajectories over areas with the lowest chance of possible casualties should be preferred. On the other hand, the longer the trajectory is, the higher chance of a crash is. Therefore, the least risky trajectory needs to be found, and an emergency landing must be guaranteed to prevent a crash in the case of LoT.

Both risk-aware trajectory planning and safe emergency landing guarantee reduce the risk induced by in-flight failure, but only partially. The risk-aware planning mitigates the consequences of an in-flight failure leading to a crash, but the aircraft may crash even in the case of LoT. On the contrary, a safe emergency landing guarantee assures a safe landing in the case of LoT, and thus eliminates the risk induced by LoT entirely. However, the consequences of the total failure are not mitigated at all. The herein studied problem combines those two approaches, and is visualized in Fig. 1. The goal is to plan trajectory minimizing the risk induced by an inevitable crash, while an option of safe emergency landing is guaranteed for failures allowing an emergency landing, such as the herein addressed LoT.

The rest of the paper is organized as follows. An overview of the related work is provided in the next section. The formal definition of the studied problem is given in Section III, with the proposed method described in Section IV. The empirical evaluation of the proposed solution is presented in Section V, and the conclusion and final remarks are in Section VI.

II. Related Work

The studied *Risk-Aware Trajectory Planning with Safe Landing Guarantee* problem combines four challenges:

The authors are with the Faculty of Electrical Engineering, Czech Technical University in Prague, Technická 2, 166 27 Prague, Czech Republic {slamajak|vanapet1|faiglj}@fel.cvut.cz

The presented work has been supported by the Czech Science Foundation (GAČR) under the research project No. 19-20238S. The support of the Ministry of Education Youth and Sports (MEYS) of the Czech Republic under project No. LTAIZ19013 is also acknowledged.

1) to satisfy the aircraft motion constraints;
2) to select a landing site and a corresponding emergency landing trajectory in the case of LoT;
3) to determine trajectory risk induced by the possible crash;
4) and to determine a trajectory minimizing the risk.

To the best of the authors' knowledge, none of the existing approaches address all the challenges. Thus, an overview of related existing works for each challenge is presented.

The aircraft motion constraints can be addressed by the Dubins airplane model [7] utilized as a simplified model for maneuver generation. The model is a three-dimensional extension of Dubins vehicle [8] allowing abrupt changes in pitch and roll angles motivated by the fact that in several cases, these angles can be changed significantly faster than the yaw angle. The model is further modified to fit the properties of small UAVs in [9]. Generation of length-efficient three-dimensional maneuvers satisfying vehicle maximum curvature and limited pitch angle is further studied in [10], and the so-called Dubins-Hélix model is introduced in [11]. A trajectory consists of spiral (hélix) segments allowing a projected turning radius into the horizontal plane to be smaller than the minimum turning radius. Thus, the final trajectory is shorter than using the Dubins airplane model [7]. However, Dubins-Hélix model [11] pushes the aircraft to its limits due to sharp turns during altitude changes. Alternatively, the trajectory generation problem can be addressed using parametric curves such as Bézier [12], [13] or B-spline curves [14]. Regarding the addressed planning problem, any of the mentioned methods can be utilized depending on the constraints of the utilized vehicle. However, high computational requirements can be expected for the herein addressed complex planning problem. Therefore, we opt for the already utilized Dubins airplane [7] that can be eventually substituted by more demanding methods in further studies.

Emergency landing can be performed in in-flight LoT, assuming a landing site is within the gliding range. A particular landing site and a landing trajectory need to be selected in such a case. A method for their selection based on the maximization of the altitude reserve is proposed in [6]. The method has been extended for multi-goal trajectory planning in [15], where the final trajectory visits all the given regions while guaranteeing a possible safe emergency landing in the case of LoT for any point of the trajectory. If a target region cannot be visited due to violation of safe altitude, a relaxed problem can be utilized where a feasible and safe solution is found using a safe altitude at which the region is visited that is higher than the originally requested unsafe altitude. Path planning for an emergency landing in LoT, assuming the landing site is within range, is further described in [16].

If the emergency landing is not possible, the in-flight failure leads to a crash inducing a risk of casualties and material loss on the ground. A precise impact location cannot be predicted, and a stochastic model has to be used for the uncontrolled fall of the aircraft [17]. The induced risk may be defined in various ways, from economic to casualties count. The authors of [2] proposed to assume risk to people, ground vehicles, and aircraft for small UAVs ground risk map; buildings are omitted due to the low impact energy of such UAVs. However, the assumed simplification counts on uniform distribution of people, ground vehicles, and aircraft on the ground. The risk as a probability of three consecutive events is proposed in [3] as (i) loss of control with an uncontrolled crash on the ground; (ii) impact with someone; and (iii) casualty of the hit person. Building a ground risk map from multiple layers is proposed in [18], where the overall risk can be determined considering different population density and sheltering factors given by buildings for different loss of control events. A type of event significantly influences the risk map based on the reported results.

Finally, various approaches can be utilized to plan the least risky trajectory. Utilization of the risk map in risk-based trajectory planning has been shown in [18]. The authors propose to evaluate the risk of a trajectory as a sum of risks of flown-over areas. The work is further adopted in [19], where the trajectory risk definition is utilized in therein proposed RiskA* algorithm to find the trajectory with the minimal risk. Both approaches utilize a pre-computed risk map for a static environment, and they are limited to a fixed flight altitude. On the contrary, online evaluation of the risk and usages of the risk-based RRT* algorithm is proposed in [20], but fixed flight level and speed are still assumed.

The current risk-aware trajectory planning approaches [18], [19], [20] allow a risk minimization for a fixed flight level, but risk mitigation by the guarantee of a safe emergency landing in LoT is not considered at all. Based on the accident investigations [4], [5], LoT is more likely to happen than a total failure of the aircraft. Thus, the elimination of risk induced by LoT could significantly reduce the overall flight risk. On the contrary, methods [6], [15] for safe landing guarantee in LoT optimize the trajectory for the LoT scenario and they do not consider any other types of failure. Hence, the herein studied problem aims to minimize the risk by both approaches simultaneously. The solution is based on approaches for emergency landing guarantee to eliminate the risk induced by possible LoT, and methods for risk-aware planning are extended for the usage of various flight levels and used for mitigation of risk induced by failures other than LoT. Both approaches are combined in the proposed solution, while the efficiency for near real-time planning is tackled.

III. Problem Statement

The studied *Risk-Aware Trajectory Planning with Safe Landing Guarantee* problem stands to find a least risky trajectory with a guaranteed safe emergency landing in the case of accidents allowing gliding to the nearby landing sites. The addressed point-to-point trajectory planning problem consists of four identified challenges.

First, it is requested that the planned trajectory **satisfies motion constrains** of the considered fixed-wing aircraft modeled as Dubins airplane [7]. The vehicle configuration q consists of its position $(x, y, z) \in \mathbb{R}^3$, heading angle $\theta \in \mathbb{S}$, and pitch angle $\psi \in \mathbb{S}$; thus $q = (x, y, z, \theta, \psi)$ and the configuration space is $\mathcal{C} = \mathbb{R}^3 \times \mathbb{S}^2$. The state of the vehicle

of the Dubins Airplane model can be described as

$$\begin{bmatrix}\dot{x}\\ \dot{y}\\ \dot{z}\\ \dot{\theta}\end{bmatrix} = v\begin{bmatrix}\cos\theta\cos\psi\\ \sin\theta\cos\psi\\ \sin\psi\\ u_\theta\rho^{-1}\end{bmatrix}, \tag{1}$$

where the vehicle forward velocity is v, the control input $u_\theta \in [-1,1]$ changes the heading angle θ, and ρ denotes the minimum turning radius. In Dubins Airplane, the pitch angle ψ is assumed to change significantly faster than θ, and the model allows abrupt changes of ψ, but its value must be within limits $\psi \in [\psi_{\min}, \psi_{\max}]$. Besides, obstacles can be within the vehicle's operational space. Therefore, obstacles $\mathcal{O}$ are considered, and the vehicle trajectory is planned in the collision-free part of the configuration space denoted $\mathcal{C}_{\text{free}}$.

The second and third challenges are to *determine a risk of the trajectory* induced by possible malfunction and to *determine the least risky trajectory*. Both challenges combined can be defined as to **minimize the risk to people on the ground** induced by a possible in-flight loss of control over the aircraft. A point-to-point trajectory $\Gamma : [0,T] \to \mathcal{C}_{\text{free}}$ from $q_i \in \mathcal{C}_{\text{free}}$ to $q_f \in \mathcal{C}_{\text{free}}$ (for $\Gamma(0) = q_i$ and $\Gamma(T) = q_f$) has the induced risk $\mathcal{R}$ given as

$$\mathcal{R} = p_{\text{fail}} \int_0^T \mathcal{M}\left(\Gamma(t)\right) \,\mathrm{d}t\,, \tag{2}$$

where p_{fail} is the probability of losing the control and $\mathcal{M} : \mathcal{C}_{\text{free}} \to \mathbb{R}$ is a function quantifying the risk at the given configuration. If a malfunction happens at $q_m \in \mathcal{C}_{\text{free}}$, the aircraft falls along a ballistic curve $\Gamma_{\text{bal}} : [0,1] \to \mathcal{C}_{\text{free}}$, s.t. $\Gamma_{\text{bal}}(0) = q_m$, until it crashes into the ground [17]. The uncontrolled fall can be described by the motion equation

$$m\dot{\boldsymbol{v}} = m\boldsymbol{g} - \frac{1}{2}c\rho S\|\boldsymbol{v}\|\boldsymbol{v}\,, \tag{3}$$

where $m\boldsymbol{g}$ denotes the gravity vector and $\frac{1}{2}c\rho S\|\boldsymbol{v}\|\boldsymbol{v}$ denotes Newton's drag force. The impact poses a risk to people on the ground, and the amount of risk is dependent specifically on the impact location and impact energy. However, parameters of (3), especially of the drag force, are saddled with uncertainties, and so the precise impact location cannot be predicted. Instead, an impact probability $p_{\text{imp}} : \mathbb{R}^2 \to \mathbb{R}$ can be found. An example is visualized in Fig. 2.

A risk $\mathcal{M}(q)$ at any configuration q is therefore given as

$$\mathcal{M}(q) = \int_{\mathbb{R}^2} p_{\text{imp}}\left(\boldsymbol{x}|\Gamma_{\text{bal}}\right) M\left(\boldsymbol{x}, E, \gamma\right) \,\mathrm{d}\boldsymbol{x}\,, \tag{4}$$

where $M\left(\boldsymbol{x}, E, \gamma\right)$ is the ground risk quantifying the possible damage with respect to (w.r.t.) the impact location $\boldsymbol{x}$, impact energy E, and impact angle γ. Determination of the ground risk M follows [18] where a probability of casualty is the result of three independent phenomena: (i) probability of failure p_{fail}; (ii) probability of hitting a person p_{hit}; and (iii) probability of casualty p_{casualty} if a person is hit. In our work, the ground risk is defined as the probability of casualty if the malfunction happens

$$M\left(\boldsymbol{x}, E, \gamma\right) = p_{\text{hit}}(\boldsymbol{x}, \gamma)\, p_{\text{casualty}}(\boldsymbol{x}, E)\,. \tag{5}$$

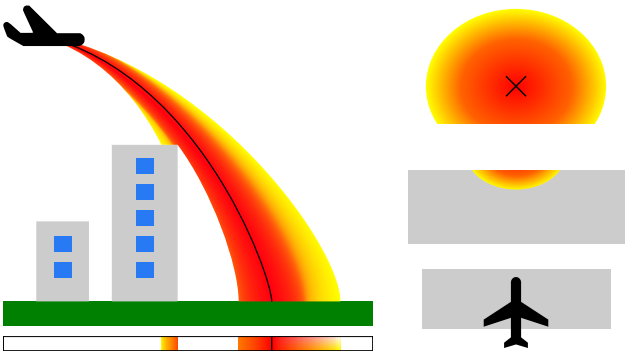

(a) Vertical slice of ballistic fall (b) Horizontal view of p_{imp}

Fig. 2. An example of ballistic fall and related impact probability. The predicted fall (black line) and the probability of the aircraft occurrence are in (a), resulting impact probability is shown in (b) (highest probability in red, the lowest one in yellow). The gray rectangles represent buildings.

The probability p_{hit} is adopted from [18] and it is given as

$$p_{\text{hit}}(\boldsymbol{x}, \gamma) = \rho(\boldsymbol{x}) A_{\text{exp}}(\gamma)\,, \tag{6}$$

where $\rho(\boldsymbol{x})$ is the population density at the impact location $\boldsymbol{x}$, and $A_{\text{exp}}(\gamma)$ is the area exposed to the crash defined as

$$A_{\text{exp}}(\gamma) = 2(r_p + r_{\text{uav}})\frac{h_p}{\tan(\gamma)} + \pi(r_p + r_{\text{uav}})^2 \tag{7}$$

with r_p and h_p denoting the radius and height of an average person, respectively, and r_{uav} is the radius of the aircraft. The probability of casualty is also adopted from [18] as

$$p_{\text{casualty}}(\boldsymbol{x}, E) = \frac{1-k}{1-2k+\sqrt{\frac{\alpha}{\beta}}\left(\frac{\beta}{E}\right)^{\frac{3}{S(\boldsymbol{x})}}}\,, \tag{8}$$

where $k = \min\left(1, \left(\frac{\beta}{E}\right)^{\frac{3}{S(\boldsymbol{x})}}\right)$, $S(\boldsymbol{x})$ denotes a shelter factor at location $\boldsymbol{x}$, α is the impact energy needed to achieve $p_{\text{casualty}} = 50\%$ when $S = 6$, and β is the impact energy causing a casualty for $S \to 0$. As proposed in [21], the value of $\beta = 34$ J is utilized.

The last challenge being addressed is to **guarantee a safe emergency landing** in LoT [15]. Let assume that m landing sites exist with touch-down configurations $\Xi = [\xi_1, \ldots, \xi_m]$. An emergency landing trajectory $\Gamma_{\text{LoT}} : [0,1] \to \mathcal{C}_{\text{free}}$ must exist from any point τ along the trajectory Γ, i.e., $\forall\tau \in [0,T] : \Gamma_{\text{LoT}}(0) = \Gamma(\tau)$, to consider the trajectory Γ as safe w.r.t. guaranteed safe emergency landing. The emergency landing trajectory is further required to end at a particular landing site $\xi_j \in \Xi$ or above it. Thus, $\Gamma_{\text{LoT}}(1)$ is from the set $\hat{\xi}_j$ of all configurations above the landing site ξ_j. The emergency landing trajectory is allowed to end above the landing site because an excessive altitude can be quickly lost by specific procedures, even in LoT [6]. An example of safe landing determination is given in Fig. 3.

The four described challenges are combined in the herein studied risk-aware point-to-point trajectory planning with a safe emergency landing guarantee. The goal is to find a feasible, least risky trajectory from some initial configuration q_i to a final configuration q_f so that the option of a safe

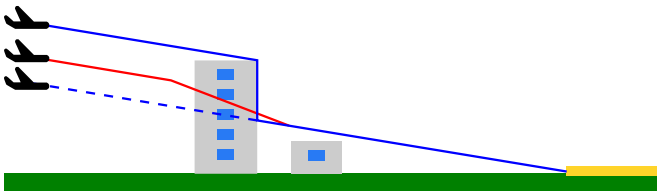

Fig. 3. An example of finding a safe emergency landing adopted from [15]. Buildings (gray) block a direct landing (dashed blue line) to the landing site (yellow). The height of flown-over obstacles influences the minimum safe altitude for a direct flight to the site (solid blue line). Flying around obstacles (solid red line) can lower the needed altitude for a safe landing.

emergency landing in the case of LoT is guaranteed for the whole trajectory. The problem can be formally defined as Problem 3.1, where the determination of the least risky trajectory is assured by (9), and (11) requires the existence of a safe emergency landing trajectory Γ_{LoT} from any point along the final trajectory Γ assuring the safe emergency landing guarantee. The final trajectory Γ is required to satisfy (1) to fulfill the vehicle motion constraints.

Problem 3.1 (Risk-Aware Trajectory Planning with Safe Emergency Landing Guarantee)

$$\min_{\Gamma} \int_0^T \mathcal{M}\left(\Gamma(t)\right) \mathrm{d}t \tag{9}$$

$$\text{s.t.} \qquad \Gamma(0) = q_i,\, \Gamma(T) = q_f \tag{10}$$

$$\forall \tau \in [0,T]\,,\ \exists \Gamma_{\mathrm{LoT}},\, \exists \xi_j \in \Xi : \tag{11}$$

$$\Gamma_{\mathrm{LoT}}(0) = \Gamma(\tau) \wedge \Gamma_{\mathrm{LoT}}(1) \in \hat{\xi}_j$$

IV. Proposed Method

The proposed solution of the risk-aware trajectory planning with safe emergency landing guarantee is based on [20] that is enhanced to assume various flight levels and to decrease trajectory risk by exploiting safe gliding trajectories to landing sites in LoT [6]. The key idea is to grow a roadmap from the final configuration q_f towards the initial configuration q_i until a trajectory is found. Hence, the risk is defined as a risk-to-goal that allows reusing the roadmap in replanning during the flight. The method is summarized in Algorithm 1, and it is described in detail in the following part.

A. Risk-based RRT* Method with Safe Emergency Landing

The initial step of the algorithm is to create a map of safe altitudes. Its creation is adopted from [15], and it is based on determining possible landing trajectories using the RRT*-based algorithm. The initial step is detailed in Section IV-B. Once the map is determined, the trajectory planning starts with the initialization of the G by the goal configuration q_f and continues by generating random sample q_{rand} as follows.

The closest node of q_{rand} in the roadmap G is extracted by the `Nearest` routine. If the sample q_{rand} extends G by more than the allowed growing step Δ_{step}, the connection is shortened, and the new sample q_{new} is created in the `Steer` routine. Afterwards, a set Q_{near} of k nearest neighbors of q_{new} is extracted by the `Near` routine. The best parent q_*

Algorithm 1: Proposed risk-based RRT* algorithm for finding the least risky trajectory and safe emergency landing (inspired by [20])

Input: q_i – Initial configuration of the aircraft
Input: q_f – Final configuration of the aircraft
Input: $\mathcal{T}_{\mathrm{alt}}$ – Altitude of the terrain (or obstacles)
Input: $\mathcal{Z}$ – Map of no-flight zones
Output: Γ – The least risky trajectory
Output: $\mathcal{R}(q_i)$ – Risk of trajectory Γ

1 $G_l, \mathcal{A} \leftarrow$ `SafeLandingMap`$(\Xi, \mathcal{T}_{\mathrm{alt}})$
2 $G \leftarrow \{\boldsymbol{V} \leftarrow q_f, \boldsymbol{E} \leftarrow \emptyset\}$
3 $\mathcal{R}(q_f) \leftarrow 0$
4 **do**
5 $\quad q_{\mathrm{rand}} \leftarrow$ `SampleUniform`$()$
6 $\quad q_{\mathrm{nearest}} \leftarrow$ `Nearest`(q_{rand}, G)
7 $\quad q_{\mathrm{new}} \leftarrow$ `Steer`$(q_{\mathrm{nearest}}, q_{\mathrm{rand}})$
8 $\quad Q_{\mathrm{n}} \leftarrow$ `Near`(q_{new}, G)
9 $\quad q_* \leftarrow \mathrm{argmin}_{q_{\mathrm{n}} \in Q_{\mathrm{n}}} \left[\mathcal{R}(q_{\mathrm{n}}) + \mathcal{R}(q_{\mathrm{new}}, q_{\mathrm{n}})\right]$
10 $\quad \mathcal{R}(q_{\mathrm{new}}) \leftarrow \mathcal{R}(q_*) + \mathcal{R}(q_{\mathrm{new}}, q_*)$
11 $\quad$ **if** `isAdmissible`$((q_{new}, q_*), G_l, \mathcal{A}, \mathcal{T}_{\mathrm{alt}}, \mathcal{Z})$ **then**
12 $\quad\quad \boldsymbol{V} \leftarrow \boldsymbol{V} \cup \{q_{\mathrm{new}}\}$; $\boldsymbol{E} \leftarrow \boldsymbol{E} \cup \{(q_*, q_{\mathrm{new}})\}$
13 $\quad\quad G \leftarrow$ `Rewire`(Q_{n}, G)
14 **while** $\|q_{\mathrm{new}} - q_i\| < \Delta_{\mathrm{tol}}$
15 $Q_{\mathrm{n}} \leftarrow$ `Near`(q_i, G)
16 $q_* \leftarrow \mathrm{argmin}_{q_{\mathrm{n}} \in Q_{\mathrm{n}}} \left[\mathcal{R}(q_{\mathrm{n}}) + \mathcal{R}(q_i, q_{\mathrm{n}})\right]$
17 $\mathcal{R}(q_i) \leftarrow \mathcal{R}(q_*) + \mathcal{R}(q_i, q_*)$
18 **if not** `isAdmissible`$((q_i, q_*), G_l, \mathcal{A}, \mathcal{T}_{\mathrm{alt}}, \mathcal{Z})$ **then**
19 $\quad$ **goto** Line 4
20 $\Gamma \leftarrow$ `ExtractTrajectory`(q_i, G)
21 **return** $\Gamma, \mathcal{R}(q_i)$

leading to the minimal risk $\mathcal{R}(q_{\mathrm{new}})$ is determined by evaluating all possible connections between the new sample and nodes in Q_{near} (Lines 9 and 10, Algorithm 1). With a slight abuse of notation, let us refer to $\mathcal{R}(q)$ as the total risk of the whole trajectory from q to q_f while $\mathcal{R}(q_1, q_2)$ denotes the risk between q_1 and q_2. An infinite risk is assumed for inadmissible maneuvers. The admissibility of maneuver between q_{new} and its parent q_* is checked by the `isAdmissible` routine, detailed in Section IV-C, and details on the risk assessment are in Section IV-D. If the maneuver is admissible, the new sample is added to the roadmap G. Finally, a rewiring is performed in the `Rewire` routine to support asymptotic optimality of the trajectory planning [22].

New samples are inserted into G until the vicinity Δ_{tol} of the initial configuration q_i is reached. Then, q_i is inserted into G in the similar manner as q_{new}. If the connection is admissible, a trajectory Γ is extracted from the graph by the `ExtractTrajectory` routine, and the planning finishes; otherwise, it continues with the roadmap expansion.

B. Safe Altitude Map Generation

A safe altitude map $\mathcal{A}$ is needed to check maneuver admissibility. Since the safe altitude map is time-invariant and determined by the aircraft gliding capabilities, the

terrain, and the location of landing sites, it can be pre-computed for effectiveness by the RRT*-based algorithm adopted from [15].

Based on the gliding aircraft model proposed in [6], the minimum safe altitude is determined for possible emergency landing trajectories. Thus, the configuration of the aircraft is simplified to its 2D position (x, y) and heading angle θ, i.e., the simplified configuration is $\tilde{q} = (x, y, \theta)$ and the simplified configuration space is $\tilde{\mathcal{C}} = SE(2)$, which significantly reduces the computational burden. Then, the altitude of $\tilde{q}$ is assumed as the minimum altitude allowing a safe emergency landing from the position $\tilde{q}$ to any landing site from the set of landing sites Ξ. The particular minimal safe altitude is influenced by the altitude of the selected landing site, altitude loss $\mathcal{H}$ of the corresponding emergency landing trajectory Γ_{LoT}, and the terrain altitude.

The algorithm is similar to Algorithm 1, i.e., a random sample is generated and steered not to extend the graph more than the maximum growing step. A parent is found from its k nearest neighbors from the graph G_l. The altitude of the new sample $\mathcal{A}(\tilde{q}_{\mathrm{new}})$ can be given as an altitude of its parent plus the altitude loss of the particular maneuver. Although such a maneuver can collide with terrain, each sample is assumed feasible if its altitude is high enough. Thus, the altitude of new sample $\mathcal{A}(\tilde{q}_{\mathrm{new}})$ can also be given as the minimal altitude allowing a collision-free trajectory between $\tilde{q}_{\mathrm{new}}$ and its parent, i.e., the colliding maneuver is elevated until it becomes collision-free. In general, the altitude of new sample $\mathcal{A}(\tilde{q}_{\mathrm{new}})$ is the higher one of the aforementioned cases. Rewiring is performed to shorten trajectories, and the process is repeated until the given planning time elapses.

C. Maneuver Admissibility Check

Having the safe altitude map $\mathcal{A}$, admissibility of any maneuver can be tested by the `isAdmissible` routine. A maneuver is admissible if it avoids all no-flight zones and it does not violate the safe altitude. The routine is summarized in Algorithm 2. It starts with a uniform sampling of the given maneuver Γ with a sampling step d_{step}. Then, the minimum safe altitude is determined for each sample. A 2D projection $\tilde{q}$ of sample q is created, and a safe altitude at the simplified configuration $\tilde{q}$ is found. A set Q_{near} of k nearest neighbors of $\tilde{q}$ from G_l is constructed. All possible connections are evaluated, and the best one to G_l is kept. Instead of adding $\tilde{q}$ into the graph, the minimum safe altitude $\mathcal{A}(\tilde{q})$ is returned (Lines 4 to 6, Algorithm 2). The maneuver is inadmissible if any of its samples are within any no-flight zone or if their altitude is below the minimum safe altitude at their location.

D. Trajectory Risk Assessment

The key feature of risk-based trajectory planning is determining the risk of a trajectory Γ between two configurations q_1 and q_2. The risk $\mathcal{R}$ of Γ is defined by (2), and the risk of configuration $\mathcal{M}(q)$ is defined by (4). The latter is influenced by the impact probability, shelter factors, and population density in the impacted area.

Algorithm 2: Check if trajectory is admissible

Input: Γ – Trajectory to be checked
Input: G_l – Roadmap of landing trajectories
Input: $\mathcal{A}$ – Minimum safe altitudes for graph nodes
Input: $\mathcal{T}_{\mathrm{alt}}$ – Altitude of the terrain (or obstacles)
Input: $\mathcal{Z}$ – Map of no-flight zones
Output: Admissibility of trajectory Γ

1 **Function** `isAdmissible`$(\Gamma, G_l, \mathcal{A}, \mathcal{T}_{\mathrm{alt}}, \mathcal{Z})$**:**
2 **forall the** $q \in$ `SamplePath`(Γ) **do**
3 $\tilde{q} \leftarrow$ `Projection2D`(q)
4 $Q_{\mathrm{near}} \leftarrow$ `Near`$(\tilde{q}, G_l)$
5 $\tilde{q}_* \leftarrow \mathrm{argmin}_{\tilde{q}_i \in Q_{\mathrm{near}}} [\mathcal{A}(\tilde{q}_i) + \mathcal{H}(\tilde{q}, \tilde{q}_i)]$
6 $\mathcal{A}(\tilde{q}) \leftarrow \max [\mathcal{T}_{\mathrm{alt}}(\tilde{q}_*, \tilde{q}), \mathcal{A}(\tilde{q}_*) + \mathcal{H}(\tilde{q}_{\mathrm{act}}, \tilde{q}_*)]$
7 **if** $q \in \mathcal{Z}$ **or** `Altitude`$(q) < \mathcal{A}(\tilde{q})$ **then**
8 **return false**
9 **return true**

The impact probability is given by the ballistic fall and its stochastic parameters [17]. However, only the initial velocity and the fallen altitude influence the impact probability. Thus, a generic ballistic fall model can be pre-computed. The fall length is determined based on the initial altitude and surrounding terrain to get an impact probability for a malfunction at any configuration q. A corresponding impact probability map is retrieved from the generic ballistic fall model, and it is properly aligned based on the vehicle heading at the configuration under examination q.

V. Results

The proposed challenging risk-aware trajectory planning with a safe emergency landing guarantee has been evaluated in an urban scenario to demonstrate its behavior and performance. Found solutions are compared with trajectories determined by the RRT* algorithm minimizing trajectory length and with trajectories found by the risk-based RRT* minimizing the trajectory risk [20] that has been extended to allow various flight levels; none of which guarantee safe emergency landing.

If a safe landing is not guaranteed when LoT occurs, the aircraft flies straight for the time needed by the pilot to evaluate the situation, e.g., to select the landing site and begin an emergency landing. In our case, the straight flight is maintained for 15 s followed by landing towards the closest landing site. If the landing site can be reached, the risk induced by LoT is assumed to be zero. If the aircraft crashes, the risk is evaluated as in (4), and the risk induced by LoT for the whole trajectory can be quantified by (2) as for the former cases.

A map of the Prague city center from OpenStreetMap [23] is used to make the urban scenario as realistic as possible. The size of the mission area is 5 km×5 km, the terrain altitude data are obtained from [24], real population density map comes from [25], and shelter factors are from [18]. Three fictional emergency landing sites with bi-directional runways are placed in the open areas around the city. All

TABLE I

RESULTS SUMMARY. MEDIAN VALUES FROM 10 INDEPENDENT RUNS. NOTE THE RISKS ARE SHOWN IN NUMBER OF CASUALTIES.

Shortest path				Least risky path				Proposed path with LoT guarantee			
$\mathcal{L}$ [km]	$\mathcal{R}$ [$\times 10^{-5}$ cas.]	$\mathcal{R}_{\text{LoT}}$ [$\times 10^{-5}$ cas.]	t_{CPU} [s]	$\mathcal{L}$ [km]	$\mathcal{R}$ [$\times 10^{-5}$ cas.]	$\mathcal{R}_{\text{LoT}}$ [$\times 10^{-5}$ cas.]	t_{CPU} [s]	$\mathcal{L}$ [km]	$\mathcal{R}$ [$\times 10^{-5}$ cas.]	$\mathcal{R}_{\text{LoT}}$ [$\times 10^{-5}$ cas.]	t_{CPU} [s]
2.0	4.8	0.0	47.8	2.1	4.6	0.0	359.3	2.0	4.7	0.0	220.5
3.1	7.6	8.0	53.4	4.6	4.7	35.0	935.9	4.4	4.8	0.0	216.4
3.3	6.4	0.0	56.9	3.8	5.5	53.7	875.6	3.8	5.7	0.0	405.7
3.3	4.7	0.0	227.3	4.0	3.7	0.0	802.5	4.0	3.7	0.0	257.7
5.3	10.5	163.0	204.5	5.8	5.8	98.5	298.7	5.9	6.0	0.0	224.4

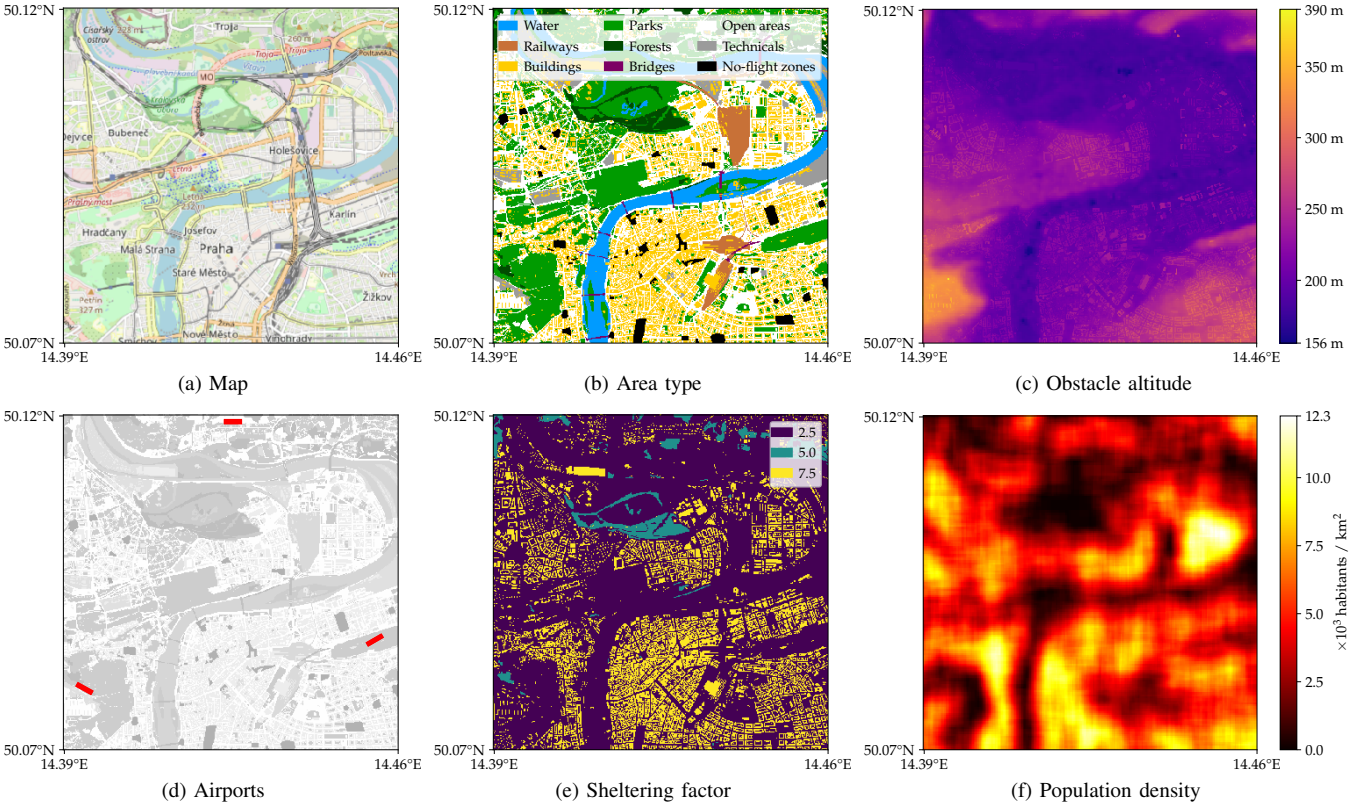

(a) Map (b) Area type (c) Obstacle altitude

(d) Airports (e) Sheltering factor (f) Population density

Fig. 4. Layers of the utilized urban scenario based on Prague city center. The map is based on the OpenStreetMap [23], altitude data are taken from [24], and a real population density [25] is used. Several fictional airports are placed around the city to simulate a realistic urban scenario.

(a) Safe altitude roadmap (b) Risk-based RRT* roadmap (c) Final trajectory

Fig. 5. An example of the found solution. The pre-computed safe altitude roadmap is depicted in (a). The roadmap of the risk-based RRT* planner is shown in (b). The resulting trajectory is presented in (c), where the population density is used as a terrain overlay. The found least risky trajectory (shown in green) is longer than the shortest trajectory (shown in blue). However, the risk of the trajectory is significantly reduced.

town squares within the map are denoted as fictitious no-flight zones simulating a ban of flights above crowds. The used mission area with all map layers is shown in Fig. 4.

Multiple instances of randomly placed initial and final configurations are evaluated for the created Prague urban scenario. The configurations are placed within the map area at the altitude in the range [300, 800] m. The aircraft model is Cessna 172 [6], one of the most used small aircraft. Real accident rate $p_{\text{fail}} = 10^{-5}\,\text{h}^{-1}$ [4] and LoT rate $p_{\text{fail}}^{\text{LoT}} = 1.3 \cdot 10^{-4}\,\text{h}^{-1}$ [5] are used. The parameters for ballistic falls are $v = \mathcal{N}(33.4, 10)\,\text{m}\,\text{s}^{-1}$, $\theta = \mathcal{N}(0, 15)°$, $\psi = \mathcal{N}(0, 15)°$, and $c = \mathcal{N}(0.7, 0.2)$, where $\mathcal{N}(\cdot, \cdot)$ denotes a normal distribution.

The created problem instances are solved by the proposed method with the following setup. The safe altitude map is

generated for 10 min resulting in a map with 5×10^3 samples and the mean distance between the samples of approximately 50 m, which is considered sufficiently dense. During the planning, each maneuver is sampled with the sampling step $d_{\mathrm{step}} = 10\,\mathrm{m}$ to check its admissibility, and the maximal roadmap growing step $\Delta_{\mathrm{step}} = 450\,\mathrm{m}$ is allowed. The final trajectory is extracted once the roadmap reaches the initial configuration within $\Delta_{\mathrm{tol}} = 450\,\mathrm{m}$.

The proposed method has been implemented in Julia ver. 1.5.3 [26] and executed on a single core of the Intel Xeon Scalable Gold 6146 CPU. Each instance has been solved ten times, and the results are summarized in Table I. An example of a solution is visualized in Fig. 5.

The results indicate that the proposed risk-based trajectory planning can significantly mitigate the risk induced by a possible malfunction. However, the resulting trajectory is prolonged w.r.t. the shortest one. Adding the safe emergency landing guarantee may further prolong the found trajectory as the safe altitude restricts the planning space. The guarantee may also slightly increase the risk induced by the total malfunction; see the results for the third instance in Table I. Nevertheless, the risk is still significantly reduced compared to the shortest trajectory. The risk induced by LoT is about one order of magnitude more significant than the risk induced by the total malfunction, as LoT is more likely to happen.

Although the LoT induced risk may be zero in specific cases, even if a safe landing is not guaranteed, the safe landing guarantee eliminates LoT induced risk in all cases reducing the whole trajectory risk. Thus, the overall risk assuming both the total malfunction and LoT is significantly reduced by the proposed method compared to the shortest and least risky trajectories without the LoT guarantee.

VI. Conclusion

In this paper, we address risk-aware trajectory planning to reduce an induced risk by possible in-flight failure. The existing approach has been extended to multiple flight levels. Besides, we address LoT when the aircraft might perform an emergency landing that can, however, result in a crash if a landing site is not within the gliding range. The proposed risk-aware trajectory planning with a safe emergency landing guarantee further reduces the risk, especially in high population density environments. The proposed method has been evaluated on a realistic urban scenario compared with shortest and risk-aware only trajectories. The provided trajectories are less risky than the shortest ones, as detours over less risky areas are preferred. Furthermore, the safe emergency landing guarantee reduces the overall risk of the final trajectory compared to the risk-aware only trajectory. Thus, the proposed method seems to be a suitable choice for trajectory planning in air urban mobility scenarios.

References

[1] M. Moore, "21st century personal air vehicle research," in *AIAA International Air and Space Symposium and Exposition: The Next 100 Years*, 2003, p. 2646.

[2] X. Hu, B. Pang, F. Dai, and K. H. Low, "Risk assessment model for uav cost-effective path planning in urban environments," *IEEE Access*, vol. 8, pp. 150 162–150 173, 2020.

[3] K. Dalamagkidis, K. Valavanis, and L. Piegl, "On integrating unmanned aircraft systems into the national airspace system, international series on intelligent systems, control, and automation: Science and engineering," *Science and Engineering*, vol. 36, 2009.

[4] J. D. Kenny, *26th Joseph T. Nall Report*. Richard G. McSpadden, JR., 2017.

[5] Australian Transport Safety Bureau, "Engine failures and malfunctions in light aeroplanes 2009 - 2014," *Investigation number AR-2013-107, 9 March 2016*, pp. 1–38, 2016.

[6] P. Váňa, J. Sláma, J. Faigl, and P. Pačes, "Any-time trajectory planning for safe emergency landing," in *IEEE/RSJ International Conference on Intelligent Robots and Systems (IROS)*, 2018, pp. 5691–5696.

[7] H. Chitsaz and S. M. LaValle, "Time-optimal paths for a dubins airplane," in *IEEE Conference on Decision and Control (CDC)*, 2007, pp. 2379–2384.

[8] L. E. Dubins, "On curves of minimal length with a constraint on average curvature, and with prescribed initial and terminal positions and tangents," *American Journal of mathematics*, vol. 79, no. 3, pp. 497–516, 1957.

[9] T. McLain, R. W. Beard, and M. Owen, *Implementing dubins airplane paths on fixed-wing uavs*. Springer Netherlands, 2014, pp. 1677–1701.

[10] P. Váňa, A. A. Neto, J. Faigl, and D. G. Macharet, "Minimal 3d dubins path with bounded curvature and pitch angle," in *IEEE International Conference on Robotics and Automation (ICRA)*, 2020, pp. 8497–8503.

[11] Y. Wang, S. Wang, M. Tan, C. Zhou, and Q. Wei, "Real-time dynamic dubins-helix method for 3-d trajectory smoothing," *IEEE Transactions on Control Systems Technology*, vol. 23, no. 2, pp. 730–736, 2014.

[12] A. A. Neto, D. G. Macharet, and M. F. Campos, "3d path planning with continuous bounded curvature and pitch angle profiles using 7th order curves," in *IEEE/RSJ International Conference on Intelligent Robots and Systems (IROS)*, 2015, pp. 4923–4928.

[13] J. Faigl and P. Váňa, "Surveillance planning with bézier curves," *IEEE Robotics and Automation Letters*, vol. 3, no. 2, pp. 750–757, 2018.

[14] E.-M. Kan, M.-H. Lim, S.-P. Yeo, J.-S. Ho, Z. Shao *et al.*, "Contour based path planning with b-spline trajectory generation for unmanned aerial vehicles (uavs) over hostile terrain," *Journal of Intelligent Learning Systems and Applications*, vol. 3, no. 03, p. 122, 2011.

[15] P. Váňa, J. Sláma, and J. Faigl, "Surveillance planning with safe emergency landing guarantee for fixed-wing aircraft," *Robotics and Autonomous Systems*, vol. 133, p. 103644, 2020.

[16] P. Eng, "Path planning, guidance and control for a uav forced landing," Ph.D. dissertation, Queensland University of Technology, 2011.

[17] A. la Cour-Harbo, "Ground impact probability distribution for small unmanned aircraft in ballistic descent," in *International Conference on Unmanned Aircraft Systems (ICUAS)*, 2020, pp. 1442–1451.

[18] S. Primatesta, A. Rizzo, and A. la Cour-Harbo, "Ground risk map for unmanned aircraft in urban environments," *Journal of Intelligent & Robotic Systems*, vol. 97, no. 3, pp. 489–509, 2020.

[19] S. Primatesta, G. Guglieri, and A. Rizzo, "A risk-aware path planning strategy for uavs in urban environments," *Journal of Intelligent & Robotic Systems*, vol. 95, no. 2, pp. 629–643, 2019.

[20] S. Primatesta, M. Scanavino, G. Guglieri, and A. Rizzo, "A risk-based path planning strategy to compute optimum risk path for unmanned aircraft systems over populated areas," in *International Conference on Unmanned Aircraft Systems (ICUAS)*, 2020, pp. 641–650.

[21] R. Standard, "321-07, common risk criteria for national test ranges. range safety group risk committee, range commanders council," *US Army White Sands Missile Range, New Mexico*, 2007.

[22] S. Karaman and E. Frazzoli, "Sampling-based algorithms for optimal motion planning," *International Journal of Robotics Research*, vol. 30, no. 7, pp. 846–894, 2011.

[23] OpenStreetMap contributors, "Planet dump retrieved from https://planet.osm.org," https://www.openstreetmap.org, 2021, accessed on: 10 Feb 2021.

[24] J. NASA, "Nasa shuttle radar topography mission global 1 arc second https://doi.org/10.5067/measures/srtm," https://opentopography.org/, 2013, accessed on: 10 Feb 2021.

[25] Facebook Connectivity Lab and Center for International Earth Science Information Network - CIESIN - Columbia University, "High Resolution Settlement Layer (HRSL). Source imagery for HRSL © 2016 DigitalGlobe," 2016, accessed on: 10 Feb 2021.

[26] J. Bezanson, A. Edelman, S. Karpinski, and V. B. Shah, "Julia: A fresh approach to numerical computing," *SIAM review*, vol. 59, no. 1, pp. 65–98, 2017.